Information transmission of mean and variance coding in integrate-and-fire neurons

Tim Herfurth and Tatjana Tchumatchenko
Max Planck Institute for Brain Research, Theory of Neural Dynamics, Max-von-Laue-Strasse 4, 60438 Frankfurt, Germany

(Received 18 December 2017; revised manuscript received 9 July 2018; published 27 March 2019)

Neurons process information by translating continuous signals into patterns of discrete spike times. An open question is how much information these spike times contain about signals which modulate either the mean or the variance of the somatic currents in neurons, as is observed experimentally. Here we calculate the exact information contained in discrete spike times about a continuous signal in both encoding strategies. We show that the information content about mean modulating signals is generally substantially larger than about variance modulating signals for biological parameters. Our analysis further reveals that higher information transmission is associated with a larger proportion of nonlinear signal encoding. Our study measures the complete information content of mean and variance coding and provides a method to determine what fraction of the total information is linearly decodable.

DOI: 10.1103/PhysRevE.99.032420

I. INTRODUCTION

The fundamental units of computation in the brain are spikes, which are binary all-or-none events generated by neurons in response to currents. These input currents reflect sensory or internal signals. For instance, these signals can modulate the average input current or vary its amplitude (see Fig. 1). How much information the spike trains carry about the arriving signals and whether variance or mean changes are more efficiently conveyed is currently an open question. evidence suggests that both mean [2–4] and variance modulation [2,3,5,6] may be present in neurons. To understand how the coding strategies of current mean modulation (MM) and variance modulation (VM) operate and which capabilities of encoding incoming signals in spikes they provide, it is crucial to determine their information coding efficiency. This question is important not only because it will help clarify intra- and cross-areal communication in the brain but because the answer to it will shed light on the basics of analog-to-binary information transmission.

A major feature of a cortical circuits across different species is a state of balanced excitatory and inhibitory inputs [7–10]. Mean modulating signals can arise from a transient imbalance between excitation and inhibition. This may be the case if excitation and inhibition are not equally tuned to a sensory stimulus [11,12] or if they are cotuned but inhibition is delayed [13–15]. In these cases, the mean somatic current in the respective neurons is modulated by the stimulus, and the net current change averaged across neurons is representative of the stimulus. For example, it has been shown in orientation-selective neurons in cat visual cortex that different orientations correspond to different levels of the average subthreshold voltages. This orientation tuning is generated by an imbalance between excitatory and inhibitory conductances [16].

In contrast, variance modulating signals may arise when excitation and inhibition are equally stimulus tuned [17] and tightly correlated at the same time [7,8,18]. In this case, external signals modulate the current and voltage fluctuations [2,19]. For instance, experimental studies in cat visual cortex have measured the power of γ-range (25–70 Hz) membrane fluctuations in response to the presentation of moving gratings in the receptive field of the considered neurons [20,21]. In this case, sensory information is encoded in the envelope of γ-band voltage fluctuations suggesting that the stimulus modifies the variability of the somatic input. A similar stimulus-tuned fluctuation strength in the θ-band (6–10 Hz) has been found in hippocampal place cells [22]. Moreover, the sensitivity to input fluctuations rather than mean changes has been shown in experimental studies on pyramidal neurons [23,24].

The properties of mean and variance modulations are often described in terms of linear response functions. These functions describe the linear filter properties of a neuron (see Ref. [25] for a review). Theoretical studies examining the leaky integrate-and-fire (LIF) and exponential integrate-and-fire (EIF) neuron models could obtain the linear response functions for mean and variance modulations analytically either over the full frequency range [26,27] or for the limit of infinitely high frequencies [28,29]; furthermore, more general semianalytic algorithms to obtain response functions were introduced [30]. The response functions generally have different functional shapes for variance and mean modulations and further depend on the spike initiation time (zero for LIF neurons and finite for EIF neurons) and steady-state characteristics [31]. In particular, for variance modulations, linear response functions in the LIF model can have finite response amplitudes even in the limit of infinitely high frequencies when white background noise is assumed [26]. This finding is supported by an *in vitro* study showing that neurons can respond to step changes in the input variance almost instantaneously [6]. For mean modulations, in contrast, white-noise background leads to a low-pass form of the linear response function [26]. This suggests that mean and variance coding strategies may use different mechanisms to convey information.

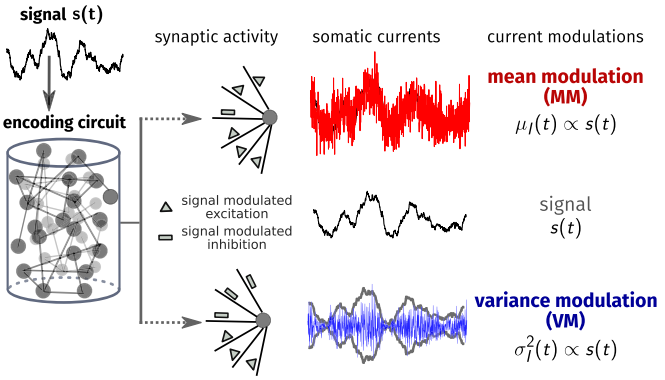

FIG. 1. Encoding signals by modulating either the mean or the variance of somatic input currents. An external signal $s(t)$ arrives at the excitatory (exc) and inhibitory (inh) neurons of an encoding neural circuit. These respond with a signal-dependent firing rate $\nu_0[1 + s(t)]$. We consider a neuron that receives inputs from this circuit. Depending on the number and type (exc vs inh) of its synaptic inputs, two cases can occur. In the first case (top, mean modulation), signal modulated exc currents are larger than their inh counterparts, thereby generating a net somatic current in individual neurons whose mean follows the signal $s(t)$ (thin red trace). In the second case (bottom, variance modulation), the exc and inh signal-modulated currents are balanced. The resulting somatic current has a signal-dependent variance (thin blue trace). Other signal-independent exc and inh inputs contribute to a background (not shown). More details can be found in Sec. III A and Sec. S1 in Ref. [1].

On the other hand, there are some similarities between the coding channels. For example, correlated noise background results in a finite amplitude of the linear response functions for both mean and variance modulations at high frequencies in the LIF model. In EIF neurons, the responses decay to zero in all cases [28]. Overall, theoretical considerations show that neural responses can have small or high-frequency cutoffs, depending on electrophysiological parameters, modulation type, and noise parameters. Experimental studies of neocortical neurons have shown that the linear response functions for both MM and VM generally have a low-pass form, but their frequency cutoffs are located at high frequencies of a few hundred hertz [2,3,32–34].

While linear response theories can anticipate the amplitude and phase of the rate response approximately, translating these findings into specific predictions about coding efficiency remains a challenge. In order to quantitatively compare mean and variance coding strategies, it is necessary to find reliable information estimates in both coding schemes. Yet the previously available information-theoretic methods have only provided a lower or upper bound for the information content [35]. The lower bound, which is computed using linear signal reconstruction, has often been used for information estimates [36–42]. However, it is still unclear how much of the total information is captured by the linear estimates used in these studies.

In the present work, we determine the exact information content of spike trains about mean and variance modulating signals in LIF and EIF neurons in the fluctuation-driven, subthreshold regime, which has been demonstrated to well describe properties of cortical activity [43,44]. Hereby we use a recently proposed method [45] to calculate the exact information content of spike trains per spike as well as a function of frequency. We perform our analysis for three different firing rates that are tuned and represented by three different noise levels. We find that spikes carry in general more information about MM signals than about VM signals when nonzero noise correlation times are assumed. Higher noise correlation times increase the information content in MM but decrease that of VM coding. Furthermore, we find that a finite spike initiation time, as incorporated in EIF models [46], limits the information containing frequency bandwidth in both modulation schemes, in agreement with linear response studies [28,30].

In order to understand the mechanisms determining information content, we compare the information per frequency with linear response functions and a measure of linearly decodable information. While we find that the linear response often serves as a proxy for the frequency filtering in the transmitted information, there are significant nonlinear effects induced by nonlinearites in the spike cross-correlation functions that escape the linear response formalism if the signal strength is increased. Finally, analyzing how much of the full information is linearly decodable, we find that the fraction of linearly encoded information is generally smaller for higher information content. However, this relation can be offset by nonlinearities at very low frequencies that occur in exponential integrate-and-fire neurons and variance coding. As another important type of nonlinear encoding we identify higher harmonics in the spike cross-correlation functions.

II. RESULTS

We consider the spike response of neurons whose input current mean or variance is modulated by the signal (see methods Sec. III A). The total mutual information $\mathcal{I}_{\text{tot}}$ about the stimulus conveyed by the resulting neural spikes is given by

$$\mathcal{I}_{\text{tot}} = -\sum_R P_R \log_2 P_R + \left\langle \sum_R P_{R|s} \log_2 P_{R|s} \right\rangle_S , \qquad (1)$$

where P_R is the probability of encountering a response R and $P_{R|s}$ is the conditional probability of encountering the response R, given that the signal s is presented. $\langle\rangle_S$ denotes the average over different signals. We can now express the mutual information $\mathcal{I}_{tot}$ as a function of angular frequency ω following the considerations in Ref. [45]:

$$\mathcal{I}_{\text{tot}}(\omega) = -\frac{1}{2} \log_2 \left[1 - \frac{C_{\text{cross}}(\omega)}{C_{\text{auto}}(\omega)} \right], \qquad (2)$$

whereby $C_{\text{auto}}(\omega)$ is the autocorrelation function of the spike trains and $C_{\text{cross}}(\omega)$ is the cross-correlation function of spike trains from different trials where the same signal was presented (see also Sec. III D). Let us note that $C_{\text{cross}}(\omega)$ is equivalent to the Fourier-transformed peristimulus time histogram (PSTH) autocorrelation function [45,47].

In our considerations, s is a stochastic signal characterized by its amplitude σ_s, its dominant, central frequency Ω_0, and its correlation time τ_s. Moreover, a stationary background noise is incorporated as an Ornstein-Uhlenbeck process parametrized by amplitude σ_n that determines the firing

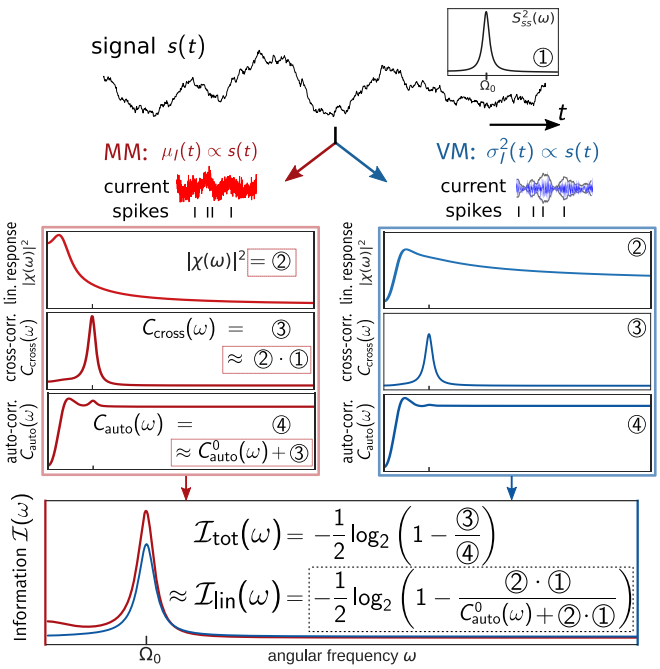

FIG. 2. Linear response theory reveals the role of response functions for information transmission. We start by considering the stimulus and its power spectrum (top). We denote the latter by ①. The signal power spectrum has a central frequency Ω_0 ($\Omega_0 = 0$ corresponds to an Ornstein-Uhlenbeck process), and its width is determined by τ_s [see Eq. (9)]. Here we show an example of a narrow signal power spectrum for illustration. Next we encode the signal in either the mean (MM left, red) or the variance of the somatic current (VM right, blue). The functions ②-④ describe the responses and their correlations evoked by mean or variance coded signals, respectively. Displayed from top to bottom are linear response function ②, linear approximation to the trial averaged spike cross-correlation function ③, and the linear approximation to the spike autocorrelation function ④. The resulting information $\mathcal{I}_{tot}(\omega)$ and its linear approximation $\mathcal{I}_{lin}(\omega)$, as given by Eq. (2) and (5), are shown for MM and VM (upper and lower curves in bottom plot). For clarity, we place boxes around the quantities we display.

rate, and correlation time τ_n ($\tau_n = 0$ means white noise; see also Sec. III B).

To uncover the functional dependencies of the mutual information, we first introduce an approximation based on linear estimates for both auto- and cross-correlation. This enables us to explore how signal features and neuronal dynamics—in particular the linear response function χ—determine the information content by means of closed-form analytical solutions (for white noise; see Fig. 2).

We start by considering the numerator in Eq. (2). Using linear kernel approximations, the cross-correlation function in the Fourier domain (③ in Fig. 2) is given by the product of the amplitude squared linear response $|\chi(\omega)|^2$ (②) and the signal power spectrum $S_{ss}(\omega)$ (①) [38,48] (see also Sec. III):

$$C_{cross}(\omega) \approx C^{lin}_{cross}(\omega) = |\chi(\omega)|^2 S_{ss}(\omega). \tag{3}$$

The relevant regions of $\chi(\omega)$ determining information transmission are given by the shape of the signal's power spectrum. To elaborate on this further, let us consider a signal power spectrum which is constant everywhere ("white"). Then, according to Eq. (3), $|\chi(\omega)|^2$ will be relevant to the information content across all frequencies. On the other hand, if the power spectrum is peaked around frequency Ω_0, then only the values $|\chi(\omega \approx \Omega_0)|^2$ will be relevant for the information content (cf. Fig. 2).

Next we address the denominator in Eq. (2). A linear approximation of the spike autocorrelation function (④) is given by [48]

$$C_{auto}(\omega) \approx C^0_{auto}(\omega) + |\chi(\omega)|^2 S_{ss}(\omega). \tag{4}$$

Here $C^0_{auto}(\omega)$ denotes the spike autocorrelation function in the absence of a signal. Note that $C^0_{auto}(\omega)$ converges to the firing rate ν_0 in this state for high frequencies $\omega \to \infty$ (cf. methods Sec. III F). Furthermore, the power spectrum $S_{ss}(\omega)$ decays with $1/\omega^2$ for large ω such that $C^{lin}_{auto}(\omega)$ also converges to ν_0 in the high-frequency limit. The influence of the signal on $C^{lin}_{auto}(\omega)$ is restricted to frequencies that are present in the signal.

The fully linearized information estimate $\mathcal{I}_{lin}(\omega)$ for the mutual information is

$$\mathcal{I}_{tot}(\omega) \approx \mathcal{I}_{lin}(\omega) = -\frac{1}{2}\log_2\left[1 - \frac{|\chi(\omega)|^2 S_{ss}(\omega)}{C^0_{auto}(\omega) + |\chi(\omega)|^2 S_{ss}(\omega)}\right]. \tag{5}$$

We recognize that in cases where $C_{cross}(\omega) \ll C_{auto}(\omega)$, we can expect to find that $\mathcal{I}_{lin}(\omega) \approx \frac{C^{lin}_{cross}(\omega)}{2C^0_{auto}(\omega)\log(2)}$, highlighting the importance of the cross-correlation function. In this linear regime (small σ_s) we can also assume that $C^{lin}_{cross}(\omega)$ is a good approximation to the cross-correlation function and basic properties of the mutual information can be derived from the properties of known linear response functions [26–30]. However, outside the linear regime nonlinear coding phenomena emerge that cannot be explained using linear responses alone (cf. Fig. 5).

For completeness, let us note that the linearly decodable information is introduced in Sec. II C. It will be used to determine the fraction of transmitted information that can be reconstructed using a linear decoder.

A. Comparing information transmission in mean and variance coding

We are now ready to analyze and compare the information content conveyed by leaky integrate-and-fire neurons via the mean and variance coding strategies. For this analysis, we quantify the full information content $\mathcal{I}^{tot} = \frac{1}{2\pi\nu}\int_0^\infty \mathcal{I}_{tot}(\omega)$ and its linear approximation $\mathcal{I}^{lin} = \frac{1}{2\pi\nu_0}\int_0^\infty \mathcal{I}_{lin}(\omega)$. These quantities represent the respective information per spike (in bits per spike). We find that the mean channel invariably outperforms the variance channel when small to moderate central signal frequencies are considered (Fig. 3). For signals with power at larger frequencies the assumption of white-noise background can change this picture in LIF neurons (see Fig. 4). The general finding holds across a broad set of signal strengths [Figs. 3(A) and 3(D)], noise strengths and firing rates [Fig. 3(B) and 3(E)], and different noise time constants [Figs. 3(C) and 3(F)]. Mean coding outperforms variance coding by as much as two orders of magnitude for

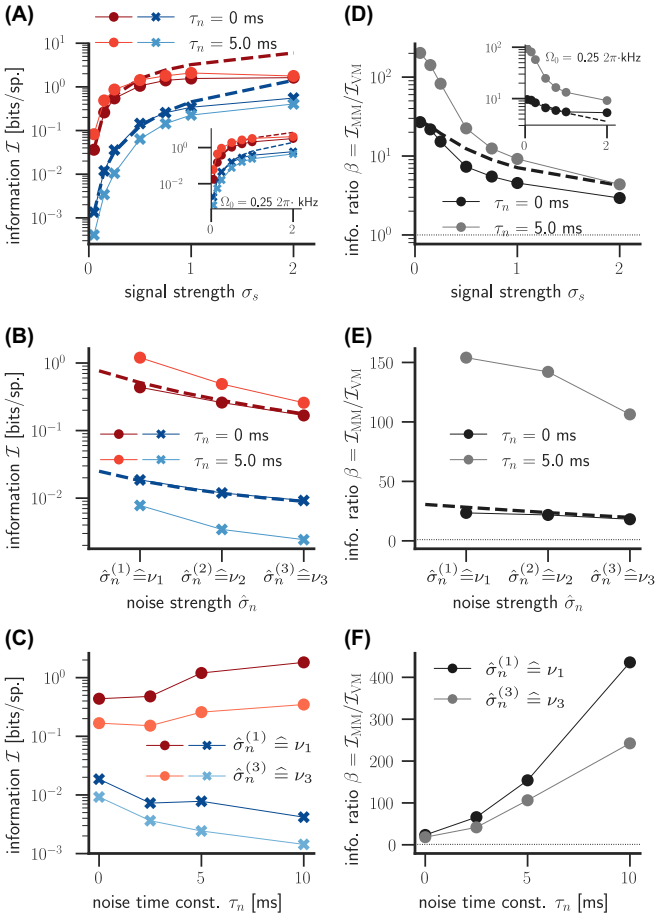

FIG. 3. Information capacity of mean and variance coding in leaky integrate-and-fire neurons. (A) Information increases monotonically as signal strength grows for both mean (MM, red circles) and variance coding (VM, blue crosses). The dashed lines denote the respective linear approximations $\mathcal{I}^{\text{lin}}$, and circles denote numerical simulations of $\mathcal{I}^{\text{tot}}$. The information is an approximation linear function of the signal strength for smaller σ_s and sublinear for larger σ_s. This finding is conserved for alternative values of the central signal frequency Ω_0 (inset). (B) Increasing the noise amplitude while keeping the signal strength constant reduces the information content for both modulations. The normalized noise strengths $\hat{\sigma}_n = \hat{\sigma}_n^{(1)}, \hat{\sigma}_n^{(2)}, \hat{\sigma}_n^{(3)}$ are increasing with equal increments and chosen to produce the three different firing rates $\nu_1 \approx 12$ Hz, $\nu_2 \approx 17$ Hz, and $\nu_3 \approx 22$ Hz for each τ_n (see Sec. III G). (C) Noise time constant τ_n has opposing effects: It reduces information for VM but increases it for MM. [(D)–(F)] The information channel ratio $\beta^{\text{tot}} = \mathcal{I}^{\text{tot}}_{\text{MM}}/\mathcal{I}^{\text{tot}}_{\text{VM}}$ (solid lines and symbols) and $\beta^{\text{lin}} = \mathcal{I}^{\text{lin}}_{\text{MM}}/\mathcal{I}^{\text{lin}}_{\text{VM}}$ (dotted lines) obtained from (A)–(C). We find that the information content is higher for MM signals across a wide parameter regime: All curves lie above $\beta^{\text{tot}} = 1$ (thin, dashed line). The information content for MM and VM becomes more similar for high σ_s and increasing noise $\hat{\sigma}_n$ [(D) and (E)]. Larger noise correlation times favor mean coding (F). We use the same color and symbol code throughout the article. For parameters, see Table I.

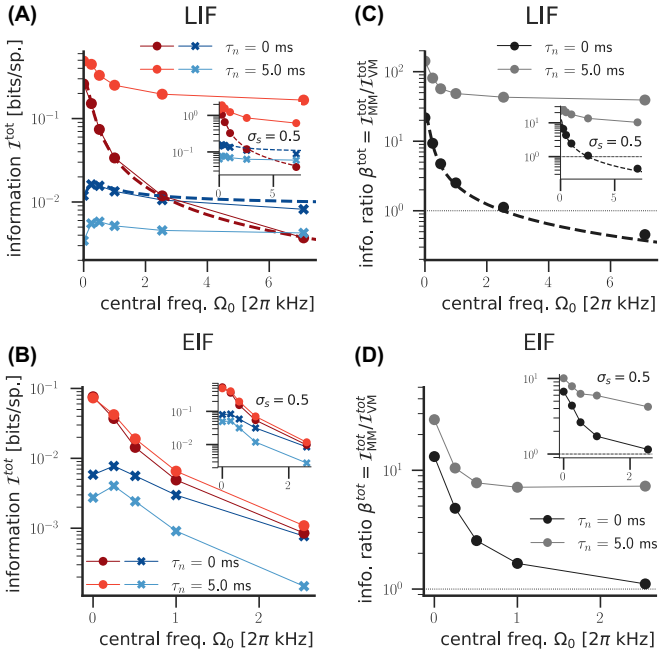

FIG. 4. Spike initiation time reduces information content for mean coding and has less effect on variance coding. (A) The information content for mean [red lines (circles)] and variance coding [blue lines (crosses)] for LIF neurons with nonwhite-noise background saturates to a finite value as the central signal frequency grows. Mean encoded information content for large signal frequencies Ω_0 and white background noise decays to zero (dashed line). (B) In EIF neurons, we also observe that mean coding has higher information content. Information content in both channels decays as the central signal frequency grows regardless of noise correlation time. Local maxima exist for VM in both LIF and EIF spiking models at small Ω_0. (C) Mean coding carries more signal information for finite noise correlation times (gray line). If the noise is white, then the ratio $\beta^{\text{tot}} = \mathcal{I}^{\text{tot}}_{\text{MM}}/\mathcal{I}^{\text{tot}}_{\text{VM}}$ will cross 1, and variance will overtake mean coding for sufficiently large Ω_0 in LIF neurons. (D) In EIF neurons, mean coding has higher information transmission regardless of noise correlation times. For both neuron models, increasing Ω_0 reduces the ratio β^{tot} and favors VM coding. Same color and symbol code as in Fig. 3.

small signal strengths [Fig. 3(D)]. For large signal strengths, the information contents of the two channels become more similar. Figure 3(B) shows that increasing noise variance (i.e., increasing firing rates) have a reducing effect on the information content in both coding strategies. This is consistent with the decay of the linear response function [Eq. (23)] for large noise strength in the MM case. However, because of previously described effects of stochastic resonance, the information is not expected to be a monotonic function of noise strength [26] and local maxima may exist. Figure 3(E) reveals that increasing noise also reduces the gap between variance and mean coding. Furthermore, we find that increasing the noise time constant strongly diminishes the information in the variance channel while boosting it in the mean channel [Fig. 3(C)]. As a consequence, we see that Fig. 3(F) reports a growing advantage of MM over VM coding for larger noise time constants. We did not find a marked dependence of the information on the signal correlation time (see Fig. S1 and S2 in Ref. [1]).

In the linear regime of small signal strengths, we find that the linear information approximation closely resembles the full information content, but for large signal strengths

the linear approximation overestimates the full information content [Fig. 3(A)]. This estimation error is mainly caused by underestimations of the firing rate and the damping of response amplitudes when the dynamic range of the rate responses becomes large (cf. Fig. S11 in Ref. [1]). Interestingly, for VM information transmission does not saturate at high signal strengths, even though a considerable overmodulation [$s(t) < -1$] can be expected to occur frequently.

B. The influence of neuronal dynamics and signal structure on information content

To investigate the impact of neuronal dynamics we use the exponential integrate-and-fire model which offers to control the spike initiation time (see method Sec. III C). We chose this model because it well fits the dynamics of cortical pyramidal neurons and stellate cells and is computationally efficient [49,50]. In Fig. 4, we present a direct comparison between the leaky and the exponential integrate-and-fire models, which we refer to as LIF and EIF, respectively. We find that the results for the EIF model generally resemble those obtained for the LIF model (cf. Fig. 9). However, EIF neurons transmit less information in the mean channel but have a similar information content in the variance channel compared to LIF neurons. Moreover, we find that crucial differences between the EIF and LIF model appear when the signal's central frequency increases.

The LIF model converges to finite information contents for large signal frequencies if the noise is temporally correlated in both the mean and variance channels [Fig. 4(A)]. However, if noise is white, then mean coding's information declines with growing frequency. This behavior is reproduced at different signal strengths [see inset to Fig. 4(A)]. This is in agreement with the fact that in the given regime the response functions of LIF neurons remain finite in the high-frequency limit [26,51]. Figure 4(C) indicates that for white-noise background in the limit of a large central signal frequency, variance modulation can be more beneficial for LIF neurons. This echoes the hypothesis by Silberberg *et al.* [6] that variance modulation evokes stronger signal encoding responses. Studying the information ratio of mean and variance coding [Fig. 4(C)] for nonwhite noise (light gray), we find that mean coding is a more efficient coding strategy by approximately two orders of magnitude.

In Fig. 4(B) and in its inset we recognize that the information content in EIF neurons declines with the central signal frequency for both mean and variance coding schemes—in accordance with the known $1/\omega$ decay of the linear response functions in both cases [28]. Interestingly, we find that mean coding still outperforms variance coding by approximately one order of magnitude [see also Fig. 4(D)], but we notice that both coding schemes become more similar as the central signal frequency increases.

Overall, we find that mean coding outperforms variance coding, except for the case of LIF neurons with white background noise and high-frequency signals. However, because postsynaptic potentials always possess finite decay times noise currents cannot be perfectly white [27]. In cases where finite correlation times in the noise are present (even if they are as small as 5 ms), we observe that mean coding provides higher information transmission also in LIF neurons. Interestingly, in the EIF model, which incorporates the finite spike initiation times as generated by the sodium channel dynamics in cortical neurons [46], we find a consistent advantage of mean over variance coding for both white and nonwhite noise. Therefore we conclude that mean coding has higher information transmission capabilities in biologically plausible settings. Comparing the values for information content and responsiveness to fast signals in LIF and EIF neurons, we emphasize the importance of spike initiation dynamics for information transmission. In particular, a finite spike initiation time introduces cutoffs for information carrying frequencies.

C. Proportion of linearly encoded information decreases with total information

The information content that can be decoded linearly is given by [35,52]

$$\mathcal{I}_{\mathrm{ld}}(\omega) = -\frac{1}{2}\log_2\left[1 - \frac{|S_{\mathrm{sr}}(\omega)|^2}{S_{\mathrm{ss}}(\omega)C_{\mathrm{auto}}(\omega)}\right] \leqslant \mathcal{I}_{\mathrm{tot}}(\omega). \quad (6)$$

Again, we define $\mathcal{I}^{\mathrm{ld}} = \frac{1}{2\pi\nu}\int_0^\infty \mathcal{I}_{\mathrm{ld}}(\omega) \leqslant \mathcal{I}^{\mathrm{tot}}$. This information estimate has been used in numerous studies [36–42] and represents a *lower bound* for the total information content [35]. It is given by the mutual information of the signal and a response-based linear signal reconstruction. Nonlinear signal-response correlations cannot be captured by Eq. (6) and are equivalent to noise from an information transmission perspective.

To assess the fraction of information that is encoded linearly, we define the information linearity index $\lambda^{\mathrm{ld}} = \frac{\mathcal{I}^{\mathrm{ld}}}{\mathcal{I}^{\mathrm{tot}}} \leqslant 1$. Figures 5(A) and 5(B) show that λ^{ld} drops with increasing signal strength in most cases and approaches 1 for vanishing σ_s. This is in line with the intuition that small signals are encoded linearly and that nonlinearities arise progressively as the signal grows. However, a crucial observation can be made: In EIF neurons, variance coding of high-frequency signals leads to local minima of λ^{ld} as a function of the signal strength [Fig. 5(B)]. For low Ω_0 the curves are found to be similar in both neuron models and share a feature: The fraction of linearly encoded information remains considerably higher when variance modulations are used rather than mean modulations. This is not an obvious finding because the signal strength σ_s in both cases equivalently describes the signal-driven modulation depth [of the input's mean or variance; see Eqs. (7) and (8)] and conceptually the linearly decodable information Eq. (6) stems from a linearization in σ_s [52].

Taking another point of view, from Figs. 5(C) and 5(D) it becomes evident that the main determinant for the linearity is given by the total information itself. Here a visualization of pooled data from both coding schemes and neuron models [(C) LIF and (D) EIF] demonstrates that data points are distributed around a decaying curve in the $\mathcal{I}^{\mathrm{tot}}$-$\lambda^{\mathrm{ld}}$ plane. Again an aberrant dependency is found for variance coding in EIF neurons at high signal frequencies (Fig. 5, light blue dots). The exceptional behavior emphasizes the importance of the spike initiation time for the responsiveness of neurons to high frequencies and is analyzed in more detail in Figs. 6(B) and 6(D). For LIF neurons, higher signal frequencies generally decrease the linearity (at a given information) in mean coding and

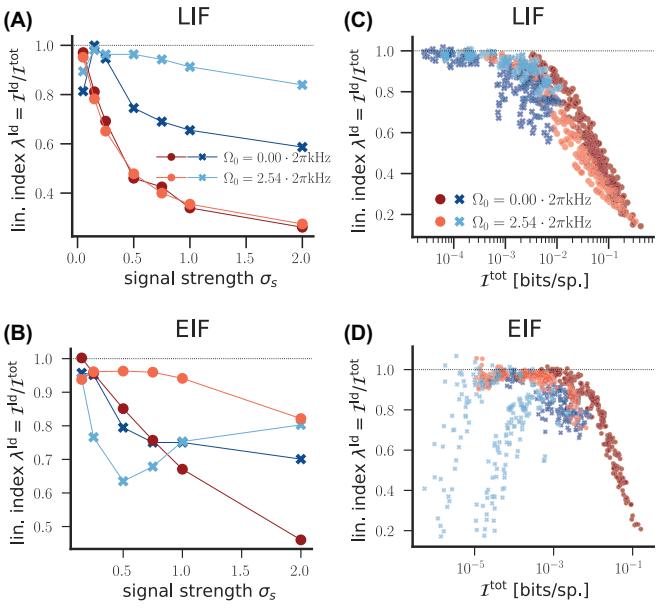

FIG. 5. Linearity of encoding is a function of the total information. The fraction of linearly decodable information is measured by $\lambda^{ld} = \mathcal{I}^{ld}/\mathcal{I}^{tot}$. (A) As a function of increasing signal strength the deviations from linearity increase faster for mean coded (MM, red circles) than for variance coded signals (VM, blue crosses) in LIF neurons. (B) The situation is different for EIF neurons. As shown here, for VM the fraction of nonlinearly encoded information can be a nonmonotonic function of the signal strength. For MM the curves are similar to those in LIF neurons. [(C) and (D)] Many simulated data points are shown together (see Table I). The two different values for the central signal frequency Ω_0 are shown as different shades of red circles and blue crosses. For LIF neurons, the linearity λ^{ld} is predominantly a function of the total information $\mathcal{I}^{tot}$ that appears to be the same for MM and VM (circles and crosses). The effect of increased central signal frequencies tends to be opposite for VM and MM: Higher frequencies (lighter colors) increase λ^{ld} in variance coding and decrease it in mean coding (C). For EIF neurons, high values of Ω_0 are related to clear reductions of the linearity λ^{ld} within variance coding (D). The effect is illustrated in Fig. 6 and yields to deviations in the overall dependence of total information and its linearly decodable fraction. In all plots the thin, dashed line denotes $\lambda^{ld} = 1$ where exact information and lower bound coincide.

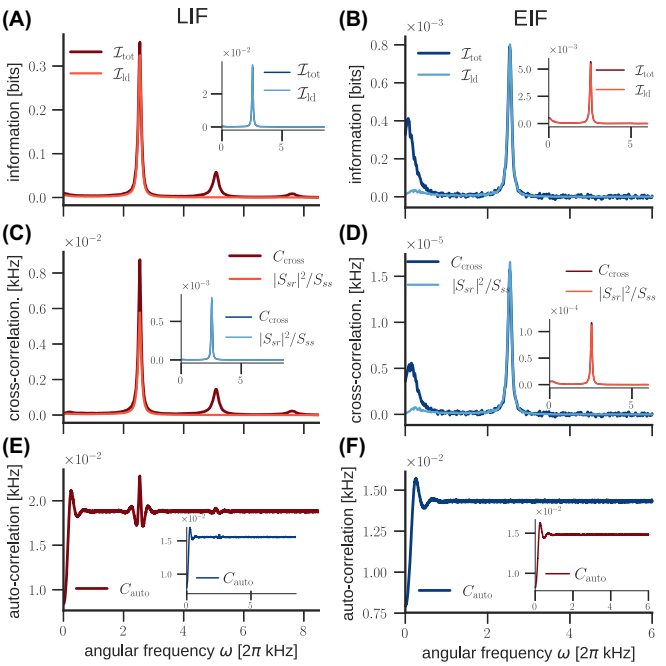

FIG. 6. Nonlinearities are observed as higher harmonics and as contributions at low frequencies. Both columns show the information-relevant, frequency-resolved functions for a rather high signal frequency $\Omega_0 = 2.54 \times 2\pi$ kHz and $\sigma_s = 0.5$. The left column represents data from LIF neurons and the right column from EIF neurons. Main plots in the left column represent MM (red) and insets corresponds to VM (blue); vice versa in the right column where insets refer to MM. (A) Nonlinearities manifest themselves in differences of the total information $\mathcal{I}_{tot}(\omega)$ (dark colors) and its linear counterpart $\mathcal{I}_{ld}(\omega)$ (light). Here nonlinearities are higher harmonics of the signal frequency and are clearly visible as local maxima at multiples of Ω_0 in mean coding. As shown in the inset, variance coding does not possess these nonlinearities at $\sigma_s = 0.5$. (B) In EIF neurons, instead of higher harmonics prominent nonlinearities are present at very low frequencies in the information for VM. Smaller contributions at these frequencies are also present in the linearly decodable information but are much smaller. For mean modulations none such nonlinearities are observable (inset). [(C) and (D)] The shape of the information and its lower bound can well be traced back to the respective cross-correlation functions. Accordingly, nonlinear contributions are reflected in differences of $C_{cross}(\omega)$ and $|S_{sr}(\omega)|^2/S_{ss}(\omega)$ (cf. Sec. III F). [(E) and (F)] The autocorrelation functions show clear signal-dependent deflections in (E) and are almost unchanged in comparison to the steady state in (F). This is in agreement with the different sizes of the cross-correlation functions in (C) and (D) that reflect the impact of the signal. The autocorrelation functions do not have much influence on the information in the shown examples. Parameters are as shown in Table I.

increase that of variance coding. In EIF neurons the effect of higher signal frequencies is generally de-linearizing, in accordance with experimental work [53,54]. Additionally, we find that larger noise amplitudes and firing rates lead to a more linear encoding (Fig. S3(A) and S3(B) of Ref. [1]), which is in line with previous reports [48,55,56]. In contrast, larger noise correlation times increase the contribution of nonlinear encoding. This effect is most pronounced in mean coding [see Figs. S3(C) and S3(D)].

D. Different types of nonlinearities are dominant in mean and variance codes

We now want to point out the origins and differences of encoding nonlinearities in mean and variance coding and the two neuron models. For this purpose we use the deviation of the total information content $\mathcal{I}_{tot}(\omega)$ and the linearly decodable information $\mathcal{I}_{ld}(\omega)$ as a nonlinearity measure—the larger the differences the more relevant are nonlinear components for information transmission at a given frequency.

We identify two major types of nonlinearities that are most prominent in different signal modulations and neuron models. For LIF neurons we find higher harmonics to be the major type of nonlinear encoding, in particular when mean modulations are used [Figs. 6(A) and 6(C)]. Here higher harmonics are contributions to the information at frequencies

that are multiples of the central signal frequency (see also in Fig. S11 in Ref. [1]) and stem from the equivalent higher harmonics in the cross-correlation function [Fig. 6(C)]. At a given signal strength higher harmonics are much stronger in MM. This is in accordance with the faster drop of λ^{ld} as a function of σ_s as shown in Fig. 5(A). However, at a given information they can be expected to be equally present in VM as Fig. 5(C) and Figs. S3(A) and S3(C) in Ref. [1] suggest.

The finite spike initiation time that is part of the exponential integrate-and-fire model gives rise to another type of nonlinearity at very low frequencies for high central signal frequencies. Contributions at low frequencies can principally be understood in a linear picture: EIF neurons are low-pass filters whose response function is highest at low frequencies. Therefore, even if the signal power is relatively small at low frequencies, the response function can compensate for that and can produce contributions to the cross-correlation at these frequencies close to 0. This gives an intuition for the origin of the small contributions to $\mathcal{I}_{\mathrm{ld}}$ and $|S_{\mathrm{sr}}(\omega)|^2/S_{\mathrm{ss}}(\omega)$ that are seen for both modulations [Fig. 6(B) and 6(D)]. However, for variance coding we also find contributions that are considerably higher than these linear ones [Fig. 6(B)]. They may be explained by higher-order interactions of similar frequencies that are each close to Ω_0 as previously described for second-order response characteristics [56]. Higher harmonics can also be observed in EIF neurons but are significant only when the total information is high.

For completeness, we also show the respective autocorrelation functions in all cases [Figs. 6(E) and 6(F)]. The size of signal-dependent modulations of the autocorrelation depends on the size of the cross-correlation. The shape of the autocorrelation seems not crucial to understand fundamental characteristics of information transmission.

III. METHODS

A. Mean and variance modulated currents

Throughout our article, we use the following definitions for the mean and variance modulated currents $I_{\mathrm{MM}}(t)$ and $I_{\mathrm{VM}}(t)$ (examples of these currents are shown in Fig. 1, and details are given in Sec. S1 of Ref. [1]):

$$I_{\mathrm{MM}}(t) = \mu[1 + s(t)] + \xi_{\sigma_n,\tau_n}(t), \tag{7}$$

$$I_{\mathrm{VM}}(t) = \mu + \sqrt{1 + s(t)}\xi_{\sigma_n,\tau_n}(t). \tag{8}$$

Here μ is a constant input current and ξ_{σ_n,τ_n} is the noise part of the current. The signal $s(t)$ has standard deviation σ_s which reflects how much the signal contributes to the current mean (for MM) or variance (for VM) relative to the steady state, and σ_s is therefore called signal strength. We further set $I_{\mathrm{VM}}(t) = \mu$ whenever $s(t) \leqslant -1$, which is equivalent to the assumption of a threshold for activation in the presynaptic encoding population. Let us give some intuition for our definitions and discuss why we think they are appropriate for the comparison between the mean and variance coding strategies. First, in the unperturbed stationary state, when no signal is present [$s(t) = 0$], both currents are equivalent [$\mu + \xi_{\sigma_n,\tau_n}(t)$]. In this state the current mean is μ and its variance is given by the variance of ξ_{σ_n,τ_n}. Second, we define the signal amplitude in MM relative to the steady-state mean μ, which gives rise to the term $\mu[1 + s(t)]$. Equivalently, the modulation of the variance relative to its steady-state value is represented by $\sqrt{1 + s(t)}\xi_{\sigma_n,\tau_n}$, whereby the square root accounts for the fact that the noise variance is modulated rather than the standard deviation.

We consider Gaussian colored noise currents $\xi_{\sigma_n,\tau_n}(t)$ that have a temporal autocorrelation $\langle \xi(t)\xi(t+h)\rangle = \frac{\sigma_n^2}{2\tau_n} e^{-|h|/\tau_n}$ with correlation time τ_n. For $\tau_n > 0$ this describes an Ornstein-Uhlenbeck process [57–59] and corresponds to the assumption of exponential synapses [29]. The limit $\tau_n \to 0$ represents instantaneous synapses and in this limit the noise current becomes Gaussian white noise with autocorrelation $\langle \xi(t)\xi(t+h)\rangle = \sigma_n^2\delta(h)$ [29]. Whenever $\tau_n = 0$ we refer to this case.

All neurons in a population receive currents modulated by the signal $s(t)$ but have individual noise sources $\xi(t)$ which are independent across trials and across neurons. We assume independent noise sources because very weak cross-correlations have been found in cortical circuits [60,61].

B. Signal properties

The signals $s(t)$ are stationary Gaussian processes with finite correlation time $\tau_s > 0$ and standard deviation σ_s. We want to emphasize that whereas Gaussian processes are a common choice, the Gaussian property is not required for the exact information calculations [45] (stationary inputs yield independent, normal distributed spike train Fourier coefficients as we show in Sec. S2 and Fig. S5 to S9 of Ref. [1]). In fact, we note that the VM current input Eq. (8) does not generally follow a normal distribution as demonstrated in Eq. (S6) of Ref. [1].

The signals' temporal structure is controlled via its power spectrum's width and height. The power spectrum is given by (depicted in Fig. 2, top)

$$S_{\mathrm{ss}}(\omega) = \left\{ \frac{\sigma_s^2\tau_s}{1 + [\tau_s(\omega + \Omega_0)]^2} + \frac{\sigma_s^2\tau_s}{1 + [\tau_s(\omega - \Omega_0)]^2} \right\}. \tag{9}$$

The maximum of $S_{\mathrm{ss}}(\omega)$ is well approximated by the central frequency Ω_0 within the range of parameters that we use (see Table I). The temporal autocorrelation function of $s(t)$ is given by

$$\langle s(t)s(t+h)\rangle = \sigma_s^2 e^{-|h|/\tau_s}\cos(\Omega_0 h). \tag{10}$$

Note that σ_s represents the standard deviation of the mean or variance modulation irrespective of τ_s.

C. Spiking models

Here we use the current based LIF and EIF neuron models to describe voltage dynamics and spike generation. Both models have proved to reproduce key properties of cortical pyramidal neurons [46,49,59]. The voltage $v(t)$ across a cell's membrane in the LIF and EIF models are given by [46]

$$\tau_m \dot{v} = -v(t) + RI(t) \tag{11}$$

and

$$\tau_m \dot{v} = -v(t) + \Delta_T \exp\left[\frac{v(t) - \theta}{\Delta_T}\right] + RI(t), \tag{12}$$

TABLE I. Signal and noise parameters used in simulations and for figures. The column *Parameter range* lists all values that were sampled in the simulations for the respective parameter. The figure columns represent the parameters that were used to produce the respective figure (sorted by subplots if present). Varied parameters used in inset figures are annotated in the plot themselves. Each $\hat{\sigma}_n^{(m)}$ was chosen to realize a fixed firing rate ν_m as explained in Sec. III G and shown in Fig. 7, 8. *This value is not included for the EIF model.

		Parameter	Fig. 3			Fig. 4		Fig. 5				
Parameter	(unit)	range	A,D	B,E	C,F	A,C	B,D	A	B	C	D	Fig. 6
σ_s	[1]	[0.05, 0.15, 0.25, 0.5, 0.75, 1, 2]	–	0.15	0.15	0.15	0.15	–	–	All but 0.05	All but 0.05	0.5
Ω_0	(2π kHz)	[0, 0.25, 0.51, 1, 2.54, 7.11*]	0	0	0	–	–	(0, 2.54)	(0, 2.54)	(0, 2.54)	(0, 2.54)	2.54
$\hat{\sigma}_n$	[1]	$[\hat{\sigma}_n^{(1)}, \hat{\sigma}_n^{(2)}, \hat{\sigma}_n^{(3)}]$	$\hat{\sigma}_n^{(2)}$	–	$(\hat{\sigma}_n^{(1)}, \hat{\sigma}_n^{(3)})$	$\hat{\sigma}_n^{(2)}$	$\hat{\sigma}_n^{(2)}$	$\hat{\sigma}_n^{(2)}$	$\hat{\sigma}_n^{(2)}$	All	All	$\hat{\sigma}_n^{(2)}$
τ_n	(ms)	[0, 2.5, 5, 10]	(0, 5)	(0, 5)	–	(0, 5)	(0, 5)	10	10	All	All	5
τ_s	(ms)	[10, 20, 30]	20	20	20	20	20	20	20	20	20	20

respectively. Here τ_m is the membrane time constant, and R denotes the cell's input resistance. The input current $I(t)$ is either mean modulated [$I_{\mathrm{MM}}(t)$] or variance modulated [$I_{\mathrm{VM}}(t)$] (see Sec. III A). All voltages are given relative to the neuron's equilibrium potential $E = 0$. In the LIF model, a spike is generated at times t_i when the membrane voltage reaches the spike threshold θ. In the EIF model, spikes are generated when $v(t)$ crosses $\theta + 50$ mV. Immediately after spiking the voltage is set to reset potential V_r in both models where it remains for a refractory period τ_r. The exponential term in Eq. (12) represents the spike initiation dynamics governed by sodium currents. In the limit of instantaneous spike generation, $\Delta_T \to 0$, the LIF and EIF models are equivalent [46].

Spike trains are expressed as $r(t) = \sum_i \delta(t - t_i)$ with firing times t_i, and the firing rate is defined as the trial or population average

$$\nu(t) = \langle r(t) \rangle. \tag{13}$$

Throughout this article we use the following parameters: $\tau_m = 10$ ms, $R = 40\,\mathrm{M\Omega}$ and $V_r = 0$ mV, $\theta = 15$ mV, in accordance with experimental findings [49,58,62]. For the LIF model, we chose $\tau_r = 0$ ms [27,51,63]. For the EIF model, it is $\tau_r = 5$ ms and $\Delta_T = 1.5$ ms [49,64].

D. Spike correlation functions

Here we introduce the spike auto- and cross-correlation functions in the Fourier domain. The autocorrelation function is given by

$$C_{\mathrm{auto}}(\omega) = \lim_{T\to\infty} \langle \tilde{r}_n(\omega)\tilde{r}_n^*(\omega)\rangle_{\mathrm{tr}_n}, \tag{14}$$

where $\tilde{r}_n(\omega)$ is the Fourier transform of the spike train in trial n. The signal and noise traces in trials $1, \ldots, N$ are independent and averaging $\langle\rangle_{\mathrm{tr}_n}$ occurs over all trials. One noteworthy property of C_{auto} is that its high-frequency limit is equal to the average firing rate, $\lim_{\omega\to\infty} C_{\mathrm{auto}}(\omega) = \nu$.

The spike cross-correlation function is defined analogously as

$$C_{\mathrm{cross}}(\omega) = \lim_{T\to\infty} \langle \tilde{r}_n(\omega)\tilde{r}_m^*(\omega)\rangle_{\mathrm{tr}_{n\neq m}}. \tag{15}$$

Here the averaging occurs over pairs of trials m and n which originate from the presentation of the same signal $s(t)$. Example correlation functions can be seen in Figs. 6 and S11 of Ref. [1]. For completeness, let us note that we use the following definition of the Fourier transform $\mathcal{F}$:

$$\mathcal{F}[f(t)] = \tilde{f}(\omega) = \int_0^T f(t)e^{-i\omega t}dt, \tag{16}$$

and define power spectra as

$$S_{xy}(\omega) = \lim_{T\to\infty} \langle \tilde{x}(\omega)\tilde{y}^*(\omega)\rangle, \tag{17}$$

in terms of the angular frequency $\omega = 2\pi f$. In the limit $T \to \infty$ of large recording lengths, the correlation functions correspond to the spike auto- and cross-spectrum, respectively.

E. Previous upper bound estimates for the mutual information

Here we recapitulate the upper bound for the frequency resolved mutual information as introduced in Ref. [35] and make an interesting observation. The upper bound is given by

$$\mathcal{I}_{ub}(\omega) = -\tfrac{1}{2}\log_2\left[1 - \gamma_{r_1r_2}(\omega)\right], \tag{18}$$

whereby

$$\gamma^2_{r_1r_2} = \lim_{T\to\infty} \frac{|\langle \tilde{r}_1(\omega)\tilde{r}_2^*(\omega)\rangle|^2}{|\langle \tilde{r}_1(\omega)\rangle|^2|\langle \tilde{r}_2(\omega)\rangle|^2}, \tag{19}$$

with spiking responses r_1, r_2 to the same signal. We identify $|\langle \tilde{r}_1(\omega)\tilde{r}_2^*(\omega)\rangle| = C_{\mathrm{cross}}(\omega)$ and $|\langle \tilde{r}_1(\omega)\rangle|^2 = |\langle \tilde{r}_2(\omega)\rangle|^2 = C_{\mathrm{auto}}(\omega)$ using standard stationarity assumptions and the relations from methods Sec. III D. Given these identities, we recognize that the upper bound Eq. (18) and exact information Eq. (2) are equivalent, $\mathcal{I}^{\mathrm{tot}} = \mathcal{I}^{ub}$, under the stationarity assumptions made for deriving Eq. (2) [45] (see Sec. S3 and Fig. S10 in Ref. [1] for more details).

F. Linear approximations to correlation functions

Assuming that the signal $s(t)$ is only a weak perturbation to the input current, we can apply linear response theory to approximate the auto- and cross-correlation functions. The dynamics of the noise averaged firing rate in the Fourier domain are then described by [48]

$$\langle \tilde{r}(\omega)\rangle_{\mathrm{noise}} = 2\pi\nu_0\delta(\omega) + \chi(\omega)\tilde{s}(\omega). \tag{20}$$

Here $\chi(\omega)$ represents the linear response functions $\chi_{\mathrm{MM}}(\omega)$ and $\chi_{\mathrm{VM}}(\omega)$ for mean modulating and variance modulation, respectively. The linear approximation to the spike cross-correlation of two neurons that share a weak signal $s(t)$ on top of a noise background is given by Eq. (3). Each spike train's autocorrelation function is approximated by Eq. (4).

Let us note here that the latter approximation does not strictly derive from the linear approximation Eq. (20) for the rate modulation [48].

Inserting Eq. (3) and (4) into Eq. (2) yields the linear information approximation $\mathcal{I}_{\rm lin}$ as given in Eq. (5). We used it to dissect the parameter dependencies of the neural information content (Figs. 2–4).

For completeness, the quantities discussed above for the LIF model with white-noise background ($\tau_n = 0$) are given by [26,51]

$$\nu_0^{-1} = \tau_m\sqrt{\pi}\int_{V_r^*}^{\Theta^*} e^{s^2}[1+\mathrm{erf}(s)]ds, \tag{21}$$

$$C^0_{\rm auto}(\omega) = \nu_0\frac{|\mathcal{D}_{i\omega\tau_m}(\Theta^*)|^2 - e^{2\delta}|\mathcal{D}_{i\omega\tau_m}(V_r^*)|^2}{|\mathcal{D}_{i\omega\tau_m}(\Theta^*) - e^{\delta}e^{i\omega t_r}\mathcal{D}_{i\omega\tau_m}(V_r^*)|^2}, \tag{22}$$

$$\chi_{\rm MM}(\omega) = \nu_0\frac{\mu}{\sigma_n}\frac{i\omega\tau_m}{i\omega\tau_m - 1} \times \frac{\mathcal{D}_{i\omega\tau_m-1}(\Theta^*) - e^{\delta}\mathcal{D}_{i\omega\tau_m-1}(V_r^*)}{\mathcal{D}_{i\omega\tau_m}(\Theta^*) - e^{\delta}e^{i\omega t_r}\mathcal{D}_{i\omega\tau_m}(V_r^*)}, \tag{23}$$

$$\chi_{\rm VM}(\omega) = \nu_0\frac{i\omega\tau_m(i\omega\tau_m - 1)}{2 - i\omega\tau_m} \times \frac{\mathcal{D}_{i\omega\tau_m-2}(\Theta^*) - e^{\delta}\mathcal{D}_{i\omega\tau_m-2}(V_r^*)}{\mathcal{D}_{i\omega\tau_m}(\Theta^*) - e^{\delta}e^{i\omega t_r}\mathcal{D}_{i\omega\tau_m}(V_r^*)}, \tag{24}$$

where $\Theta^* = \frac{(\Theta/R-\mu)}{\sqrt{2}\sigma_n}$ and $V_r^* = \frac{(V_r/R-\mu)}{\sqrt{2}\sigma_n}$ and $\mathcal{D}_a(x)$ denotes the parabolic cylinder function.

G. Numerical simulations

Here we provide details on how we generated the signal and noise traces, produced the spike trains, and obtained the correlation functions in our numerical simulations. We simulated white noise by drawing independent numbers from $\mathcal{N}(0, 1/\sqrt{\Delta t})$. To generate the traces of signal and noise for $\tau_n > 0$, we used the algorithm from Ref. [65].

Parameters were chosen to produce cortical firing statistics [43,58,66–68]. This was done by setting three different target firing rates and a target range of coefficients of variation and then tuning the parameters accordingly. In particular, we adjusted the noise strengths σ_n and μ for each noise correlation time τ_n and each neuron model such that the three different firing rates where realized by three different values of σ_n at fixed μ. Following this experiment-driven approach we obtained for each τ_n three values of σ_n corresponding to the firing rates ν_1, ν_2, ν_3 that we denote by $\hat\sigma_n^{(1)}$, $\hat\sigma_n^{(2)}$, $\hat\sigma_n^{(3)}$, respectively. These firing rates measured in the steady state are $\nu_1 = (11 \pm 1.1)$ Hz, $\nu_2 = (16.8 \pm 0.6)$ Hz, $\nu_3 = (21 \pm 0.4)$ Hz for the LIF model and $\nu_1 = (10 \pm 1.2)$ Hz, $\nu_2 = (16.3 \pm 0.8)$ Hz, $\nu_3 = (20.7 \pm 0.8)$ Hz for the EIF model. The values of the coefficient of variation are between 0.6 and 0.9. The values for σ_n and firing statistics can be found in Figs. 7 and 8. All sampled parameters and those used for the figures are given in Table I. In Table II, the numerical values of σ_n and μ at the different τ_n are listed (see also Fig. 7 and 8).

After obtaining the signal modulated currents, we next iteratively solved Eq. (11) and (12) via the Euler method with time discretization width $\Delta t = 0.02$ ms. The resulting spike times were discretized at 0.1 ms (sampling frequency 10 kHz).

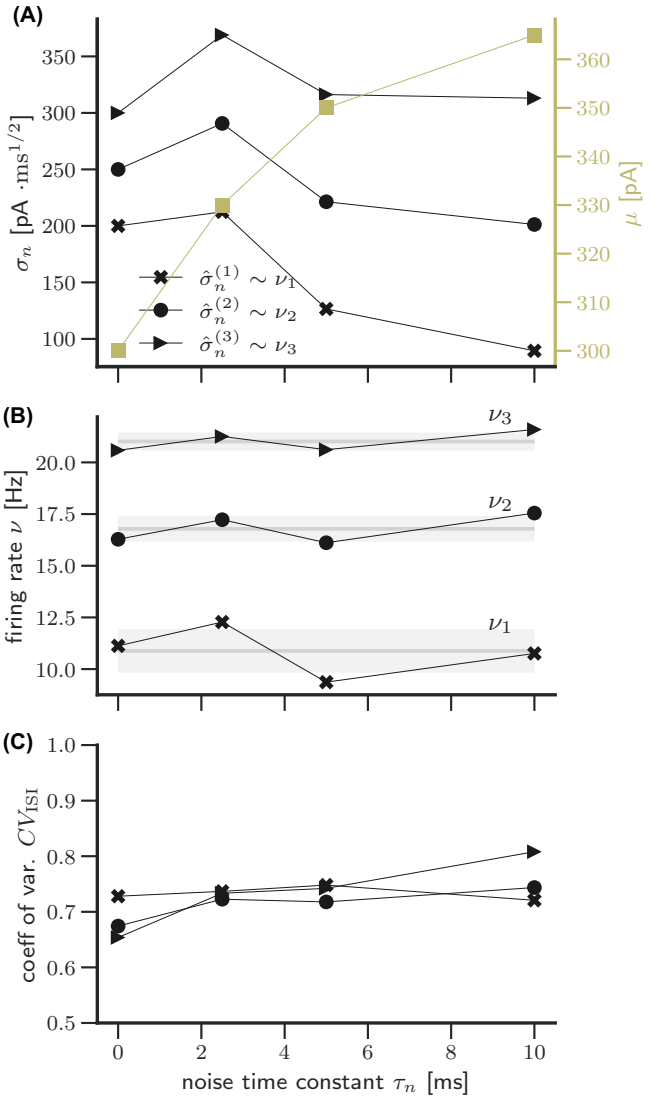

FIG. 7. Noise strength and constant input current in the LIF model were chosen to yield spiking statistics in agreement with experimentally recorded firing statistics. The spiking statistics are shown for the signal-free case ($\sigma_s = 0$). (A) For each noise correlation time τ_n one value of μ (olive squares, right axis) and three equidistant values of σ_n (different symbols, left axis) were chosen and resulted in the spiking statistics shown in (B) and (C). As follows from (B), for each τ_n one value of σ_n can be assigned to one of three firing levels. These are denoted by $\sigma_n^{(1)}$, $\sigma_n^{(2)}$, $\sigma_n^{(3)}$ (cf. Figs 3 and 5) and correspond to the firing rates ν_1, ν_2, ν_3 as explained in Sec. III G of the main article. Panel (C) confirms that all chosen parameters yield values of $CV_{\rm ISI}$ in between 0.6 and 0.8. The firing statistics are in agreement with the targeted values which are reported experimentally [43,66–68].

To obtain the spike autocorrelation function, we generated 256 000 independent spike trains of 4-s length. The autocorrelation function was calculated using Eq. (14) by averaging over all trials. To calculate the cross-correlation function, we generated 4000 trials for each of 64 different stimuli $s(t)$ with varying, independent noise trajectories (256 000 trials in total; each trial 4 s). We evaluated all pairs $|\tilde r_i^k(\omega)\cdot\tilde r_j^k(\omega)|^2$ for the same stimulus trajectory $s_k(t)$ and averaged across

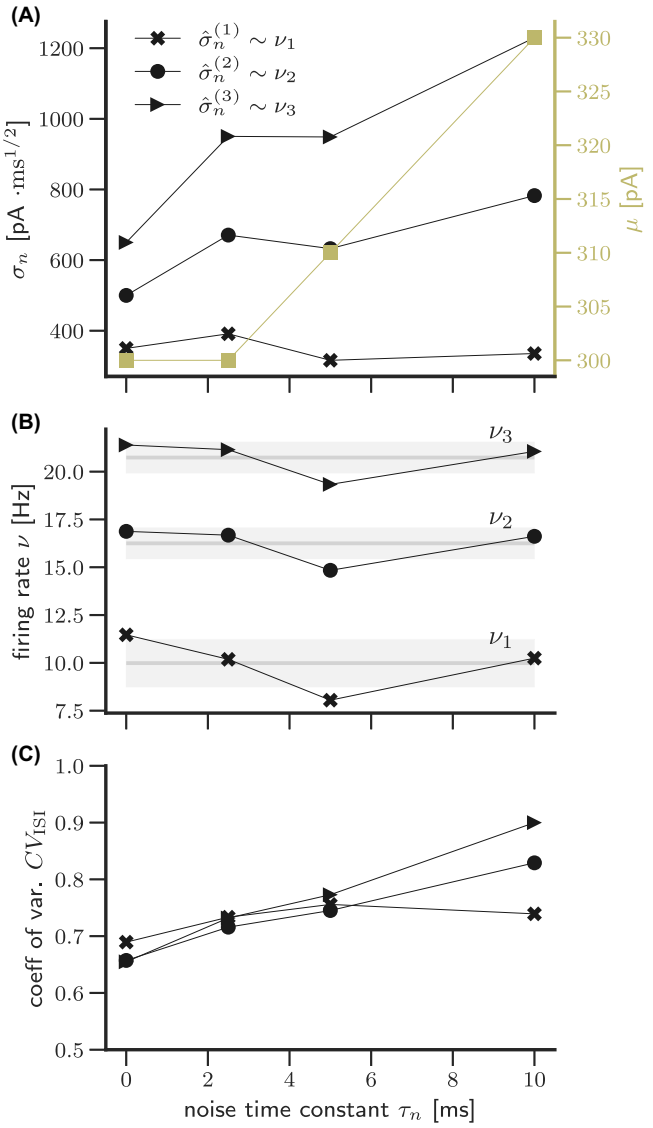

FIG. 8. Noise strength and constant input current in the EIF model were chosen to yield spiking statistics in agreement with experimentally recorded firing statistics. The spiking statistics are shown for the signal-free case ($\sigma_s = 0$). (A) For each noise correlation time τ_n one value of μ (olive squares, right axis) and three equidistant values of σ_n (different symbols, left axis) were chosen and resulted in the spiking statistics shown in (B) and (C). As follows from (B), for each τ_n one value of σ_n can be assigned to one of three firing levels. These are denoted by $\sigma_n^{(1)}$, $\sigma_n^{(2)}$, $\sigma_n^{(3)}$ (cf. Figures 9) and correspond to the firing rates ν_1, ν_2, ν_3 as explained in Sec. III G of the main article. (C) confirms that all chosen parameters yield values of CV_{ISI} in between 0.6 and 0.9. The firing statistics are in agreement with the targeted values which are reported experimentally [43,66–68].

trials to obtain $C^k_{\mathrm{cross}}(\omega)$. We repeated this procedure for all 64 independent stimuli and obtained the cross-correlation function as $\frac{1}{64}\sum_{k=1}^{64} C^k_{\mathrm{cross}}(\omega)$. All correlation functions were smoothed with a Hanning window function with a width of 5 Hz. To obtain $\mathcal{I}^{\mathrm{tot}}$ and $\mathcal{I}^{\mathrm{ld}}$, we used cutoffs of $\omega_{\max} = 3\Omega_0 + 3 \times 2\pi\,\mathrm{kHz}$ and $\omega_{\max} = 8 \times 2\pi\,\mathrm{kHz}$ in the integration over frequencies, respectively. We note that for long spike trains ($T \gg \tau_s, \tau_n$), it is equivalent to average the information content over stimuli or to first obtain the stimulus averaged cross-correlation function and then compute the respective information (we chose the latter). We used the same procedure to determine the signal-response cross-spectrum $S_{\mathrm{sr}}(\omega)$ of Eq. (6) in order to calculate the linearly decodable information by first evaluating the Fourier transforms of $s(t)$ and $r(t)$. Also let us note that the source code underlying our results is available online under [69].

TABLE II. Values of $\boldsymbol{\sigma_n}$ corresponding to $\hat{\boldsymbol{\sigma}}_{\boldsymbol{n}} = [\hat{\sigma}_n^{(1)}, \hat{\sigma}_n^{(2)}, \hat{\sigma}_n^{(3)}]$ and μ for the different $\boldsymbol{\tau_n}$. Parameters $\hat{\sigma}_n$ were chosen equidistantly and in order to produce three different, fixed firing rates at given CV_{isi} and constant input current μ. The values can also be seen in Figs. 7 and 8.

	LIF		EIF	
τ_n (ms)	$[\hat{\sigma}_n^{(1)}, \hat{\sigma}_n^{(2)}, \hat{\sigma}_n^{(3)}]$ (pA$\sqrt{\mathrm{ms}}$)	μ (pA)	$[\hat{\sigma}_n^{(1)}, \hat{\sigma}_n^{(2)}, \hat{\sigma}_n^{(3)}]$ (pA$\sqrt{\mathrm{ms}}$)	μ (pA)
0	[200, 250, 300]	300	[350, 500, 650]	300
2.5	[95, 130, 165]$\sqrt{5}$	330	[175, 300, 425]$\sqrt{5}$	300
5	[40, 70, 100]$\sqrt{10}$	350	[100, 200, 300]$\sqrt{10}$	310
10	[20, 45, 70]$\sqrt{20}$	365	[75, 175, 275]$\sqrt{20}$	330

IV. DISCUSSION

In this work, we studied the information about mean and variance modulating signals contained in spike trains. Modulations of the mean somatic current due to a transient break in the excitation-inhibition balance have been reported in a number of areas, among which are auditory, visual, and barrel cortex [11,12,14–16]. Similarly, experimental observations revealed that simultaneous modulation in the excitatory and inhibitory activity [7,8,11,17,18,21] can induce signal-dependent changes in the strength of the somatic fluctuations. The encoding of sensory or internal signals via mean or variance modulations has been addressed experimentally [3,6] and theoretically in the linear regime [2,26,63]. These studies pointed to the possibility that variance modulation may be faster or more efficient in signal encoding if it occurred on a white-noise background. However, no comparative evaluation of the information transmission properties of mean and variance coding has existed beyond the linear regime. While the experimental level has been the focus of many studies, a number of mechanistic and computational questions related to how mean and variance modulating signals are represented at the spike level have remained open. In particular: How many bits per spike are transmitted by mean and variance modulating signals? Does it make a difference whether a particular signal is encoded in the mean or variance? Is the information encoding linear?

Here we tackled these questions by calculating the mutual information between the signal and the resulting spike trains and revealed a number of features. First, mean coded signals have a larger information capacity than variance coded signals in almost all cases we considered. It is always the case when noise has temporal correlations (see Figs. 3, 4, and 9). Only if white background noise and signals with very high

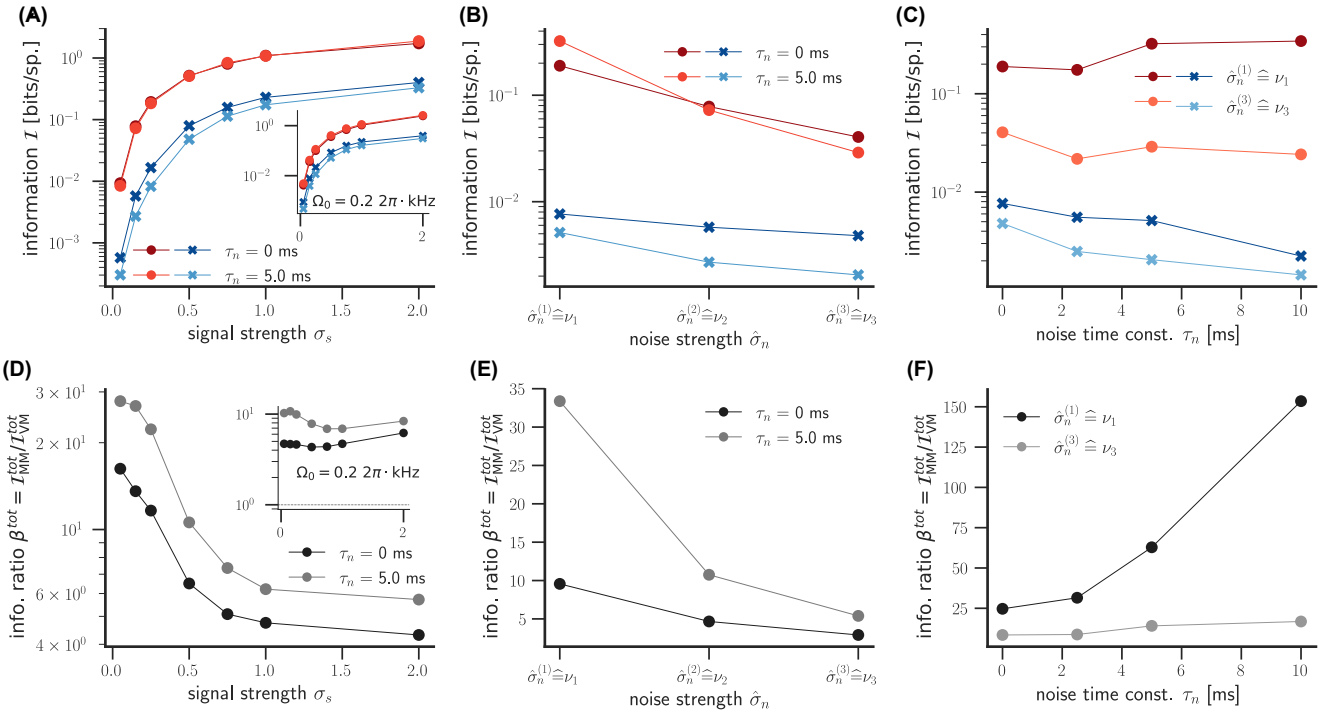

FIG. 9. Information capacity of mean and variance coding in exponential integrate-and-fire neurons. In (A), (B), and (C) information for mean coding (red circles) and variance coding (blue crosses) is shown for EIF neurons as a function of signal and noise strength and firing rate and noise correlation time (see Fig. 3 for comparison to LIF neurons). (A) Information increases monotonically as a function of the signal strength. (B) Increasing the firing rate through increased noise has a reducing effect on the information content for both modulations. (C) The effects of increasing noise correlation time are opposite for mean and variance coding: $\mathcal{I}^{tot}_{MM}$ increases with τ_n, while $\mathcal{I}^{tot}_{VM}$ decreases. [(D)–(F)] The information ratio $\beta^{tot} = \mathcal{I}^{tot}_{MM}/\mathcal{I}^{tot}_{VM}$ corresponding to (A)–(C). All curves lie above the line $\beta^{tot} = 1$ and accordingly the information transmission for MM is consistently larger than for VM. From (D) follows that mean and variance coding become more similar for high σ_s. Panel (E) indicates that variance coding is less impacted by increasing noise strength and firing rate. (F) Larger noise correlation times favor mean coding. Parameters are $\sigma_s = 0.15$ [(B) and (E), (C) and (F)], $\Omega_0 = 0$, $\hat{\sigma}_n = \hat{\sigma}_n^{(2)}$ [(A) and (D), (C) and (F)], $\tau_s = 20$ ms.

frequencies are assumed do we find an advantage of variance modulation in information transmission for LIF neurons. This is in agreement with the respective response functions [26] and with the findings of Silberberg *et al.* [6]. However, the white noise is not biologically plausible because postsynaptic potentials have finite, nonzero correlation times. Analyzing the EIF spiking model, we observed an advantage of mean coding over variance coding regardless of signal and noise parameters. It is important to note that our results are not limited to the linear regime but are valid across all considered signal strengths.

Second, our results show that variance and mean encoding are mechanistically different in the way they operate. While variance coding remains largely linear at large signal strengths, mean coding exhibits large nonlinear contributions already at small to moderate signal strengths (see Fig. 5 and 6). However, if the degree of linearity is compared at similar values of information, then one finds it to be similar for both coding schemes.

Previous work comparing the mean and variance encoding capabilities, both theoretical and analytical, has almost exclusively focused on comparing the amplitude of the respective linear response functions [2,3,6,26,30]. In this study, we computed the exact information content conveyed by the two coding channels. Using the linear theory of Eq. (5), we were able to connect features of linear response functions with information transmission capabilities (cf. Fig. 2): Linear response functions describe signal-dependent rate modulations—as measured by the PSTH—which determine the spike cross-correlation function Eq. (3) and therefore are critical to information content. We found that the response functions for leaky and exponential integrate-and-fire neurons [26,30] can often predict well the qualitative parameter dependence of information transmission even for larger signal strengths. However, the detailed functional form of the information content cannot be derived from linear responses only but can have significant nonlinear contributions, which can be captured with the exact method used in this work.

Furthermore, let us note that for this study, we chose the spiking model parameters such that the irregular spiking statistics reproduces features of cortical recordings [43,58,66–68] and selected the exponential and leaky integrate-and-fire models which have been proven to be accurate for live cortical neurons [46,49,59]. We did this to ensure that the information content we predict is relevant for the *in vivo* and *in vitro* situations encountered in experiments. As a consequence, we recover similar information values ranging from 0.1 to 10 bits/spike as in previous experimental studies [35]. We generalized these findings by exploring many "what if" scenarios by varying the firing rate, noise correlation statistics, signal strengths, and spiking mechanisms.

Experiments revealed that the statistics of the input currents, both background and signal dependent, vary considerably across brain regions and depend on the brain state [70]. This indicates that the range of time constants and other parameters that we considered is likely to be realized either in different brain states or brain regions. Differences in information content which we report may be indicative of the different computational capabilities in these brain regions. For example, our results revealed that stronger signals lead to vanishing differences between the mean and variance coding (Fig. 3). This indicates the possibility of a regime where the variety in neurotransmitter time constants [71,72] can be optimized either for maximizing the information content for either mean and variance encoding, or this content can be minimized to enable more complex information transformations. Similarly, our results in Figs. 4(A) and 4(B) indicate the existence of local optima for variance coding for specific signal frequencies. Since the location of these optima depends on neuronal spiking mechanism and background noise, they could be targeted by a brain region by enhancing those synaptic time constants from the available pool that best match the properties of the signal.

We recognize that the results of our study may differ—in particular quantitatively—when other neuron models with different response properties are considered (cf. Ref. [73]). Experimental studies suggest that neural response properties are diverse in *in vivo* and *in vitro* situations [2,3,32–34]. In particular, there is experimental work suggesting that some cortical neurons are indeed more sensitive to input fluctuations than to mean changes [23,24]. We would like to emphasize that our results can be tested *in vitro* by injecting mean and variance modulated currents with the properties of interest into current-clamped neurons. The mutual information can then be computed according to Eq. (2) from trials with repeated and varying signals.

Our results not only provide insights into the coding properties of single neurons but also can also shed light on the mechanisms of network level coding. In a recurrent network of N neurons where each neuron fulfils the stationarity and finite memory conditions the information-relevant features are represented in the $N \times N$ correlation matrix of the spike trains' Fourier coefficients of these neurons. The diagonal elements of this matrix mirror single neuron encoding which can be understood using our results. This provides a first-order approximation of how mean and variance coding strategies impact network-level coding. The off-diagonal elements which are determined by cross-neural correlations, such as noise correlations, can further reduce or increase the network's information content [47]. A fruitful direction for future studies would be to evaluate how recurrent feedback and noise correlations alter the information content in mean and variance coding.

Regarding our investigations of the linearly decodable portion of the transmitted information, we close an important gap left by previous studies. Previously, it was hard to calculate the full information content because few reliable methods existed [45]. While estimating the linear information contribution is very tractable and many studies have addressed this by means of a lower bound for the information [4,21,33,35,36,40–42], measuring the nonlinear components or the complete information content had been significantly more challenging. A procedure has been put forward to estimate the nonlinear contributions to neural coding through a linearity index defined as the ratio of the signal-response coherence $S_{\mathrm{sr}}(\omega)$ and the square root of the response-response coherence [Eq. (19)] [53,54,74]. Studies using this method indicated that an increasing signal strength leads to stronger nonlinear contributions [37,53], which is in agreement with our results, in particular for mean coding. However, measurements of the linearly encoded information content have not been attempted and the information transmission capabilities of variance encoding have not been addressed to the best of our knowledge. Furthermore, we demonstrated that an information estimate that was previously understood as an upper bound coincides with the exact information (see Sec. III E).

Our results show that variance and mean encoding have different properties regarding the linearity of the code they utilize to transmit information. The encoding linearity is mostly a function of the total information itself for both coding schemes across a wide range of time constants and signal and noise strengths (an exception being variance coding in the EIF model). However, variance coding, in contrast to mean coding, remains largely linear even for high signal strengths with an linearity index above 70% (see Fig. 5). Another difference between both the coding schemes and neuron models lies in the kind of nonlinearities that they predominantly feature. We identify higher harmonics as the major source of nonlinearities for LIF neurons. They can be observed in mean coding already at rather small signal strengths. In EIF neurons the most prominent nonlinearities are introduced at low frequencies when the signal is centered around high frequencies. This is best seen for variance modulation (Fig. 6) and probably results from the nonlinear interaction of similar frequencies present in the signal. In both coding channels, we have observed a linearizing effect of increased noise or firing rate which has been described earlier [48,53,55].

The differences of LIF and EIF models in producing nonlinearities in cross-correlation functions are based on the spike initiation mechanism. In fact, the spike initiation time Δ_T not only influences the linear response function but will also impact higher-order response functions, especially at high frequencies, that are causal for nonlinear response characteristics [56]. Our findings suggest that the finite spike initiation time of neurons can facilitate the appearance of low-frequency power in the cross-correlation function, or, equivalently, PSTH, that stems from high-frequency variance modulations. This could be an interesting starting point for the investigation of neural signals that possess low-frequency power with unknown causes.

Let us note that in a given network *in vivo*, both encoding schemes are likely used in parallel because modulations of the excitation and inhibition due to arriving signals often occur simultaneously but are not perfectly balanced [10,21]. To evaluate the neural codes used in this situation, it is necessary to assess how mean and variance modulations interact intracellularly and on the network level. For example, simultaneously recording the changes of excitatory and inhibitory inputs in nearby neurons (as in Ref. [13]) as a function of sensory inputs *in vivo* could help to assess the amount of variance and mean

coding present in the intact brain. In our present study, however, we treated mean and variance encoding individually and studied them separately. Generalizing the present results and exploring how mean and variance coding arise and interact in a recurrent network may lead to further insights into the mechanisms of neural coding.

We have provided a comprehensive analysis of mean and variance coding capabilities and assessed their linear and nonlinear components. Our work provides insight into the information transmission capacities of variance coding that have not been addressed before and shows how different parameters of the neural system influence the performance of mean and variance codes. Importantly, these results for information content are exact and therefore provide good references for future studies. The method we used to compare full and linearly decodable information is transferable to the investigation of other neural codes. In particular, they can be applied to experimental data—by evaluating the respective spike correlation functions—and do not rely on the knowledge of the specific code being used, which often is unknown.

ACKNOWLEDGMENTS

This work has been supported by the Max Planck Society, the DFG via CRC1080, and the Polytechnische Gesellschaft (T.T.). T.H. acknowledges the travel support of the Joachim Herz Foundation. We thank Andreas Nold and members of the Theory of Neural Dynamics group for helpful comments on earlier versions of this manuscript and Dooyoung Kim for proofreading.

[1] See Supplemental Material at http://link.aps.org/supplemental/10.1103/PhysRevE.99.032420 for complementing figures, mathematical details on mean and variance modulated currents, an analysis of the statistics of the spike train Fourier coefficients, and a derivation of the identity of the exact information and its upper bound.

[2] Tatjana Tchumatchenko, Aleksey Malyshev, Fred Wolf, and Maxim Volgushev, Ultrafast population encoding by cortical neurons, J. Neurosci. **31**, 12171 (2011).

[3] C. Boucsein, T. Tetzlaff, R. Meier, A. Aertsen, and B. Naundorf, Dynamical response properties of neocortical neuron ensembles: Multiplicative versus additive noise, J. Neurosci. **29**, 1006 (2009).

[4] Fred Rieke, *Spikes: Exploring the Neural Code* (MIT Press, Cambridge, MA, 1999).

[5] M. N. Shadlen and W. T. Newsome, Noise, neural codes and cortical organization, Curr. Opin. Neurobiol. **4**, 569 (1994).

[6] G. Silberberg, M. Bethge, H. Markram, K. Pawelzik, and M. Tsodyks, Dynamics of population rate codes in ensembles of neocortical neurons, J. Neurophysiol. **91**, 704 (2004).

[7] Y. Shu, A. Hasenstaub, and D. A. McCormick, Turning on and off recurrent balanced cortical activity, Nature **423**, 288 (2003).

[8] B. Haider, A. Duque, A. R. Hasenstaub, and D. A. McCormick, Neocortical network activity *in vivo* is generated through a dynamic balance of excitation and inhibition, J. Neurosci. **26**, 4535 (2006).

[9] N. Dehghani, A. Peyrache, B. Telenczuk, M. Le Van Quyen, E. Halgren, S. S. Cash, N. G. Hatsopoulos, and A. Destexhe, Dynamic balance of excitation and inhibition in human and monkey neocortex, Sci. Rep. **6**, 23176 (2016).

[10] J. S. Isaacson and M. Scanziani, How inhibition shapes cortical activity, Neuron **72**, 231 (2011).

[11] G. K. Wu, P. Li, H. W. Tao, and L. I. Zhang, Nonmonotonic synaptic excitation and imbalanced inhibition underlying cortical intensity tuning, Neuron **52**, 705 (2006).

[12] L. I. Zhang, A. Y. Y. Tan, C. E. Schreiner, and M. M. Merzenich, Topography and synaptic shaping of direction selectivity in primary auditory cortex, Nature **424**, 201 (2003).

[13] M. Okun and I. Lampl, Instantaneous correlation of excitation and inhibition during ongoing and sensory-evoked activities, Nat. Neurosci. **11**, 535 (2008).

[14] M. Wehr and A. M. Zador, Balanced inhibition underlies tuning and sharpens spike timing in auditory cortex, Nature **426**, 442 (2003).

[15] M. J. Higley and D. Contreras, Balanced excitation and inhibition determine spike timing during frequency adaptation, J. Neurosci. **26**, 448 (2006).

[16] J. S. Anderson, M. Carandini, and D. Ferster, Orientation tuning of input conductance, excitation, and inhibition in cat primary visual cortex, J. Neurophysiol. **84**, 909 (2000).

[17] M. Xue, B. V. Atallah, and M. Scanziani, Equalizing excitation-inhibition ratios across visual cortical neurons, Nature **511**, 596 (2014).

[18] A. Y. Y. Tan, S. Andoni, and N. J. Priebe, A spontaneous state of weakly correlated synaptic excitation and inhibition in visual cortex, Neuroscience **247**, 364 (2013).

[19] J. A. Cardin, L. A. Palmer, and D. Contreras, Cellular mechanisms underlying stimulus-dependent gain modulation in primary visual cortex neurons *in vivo*, Neuron **59**, 150 (2008).

[20] M. Volgushev, J. Pernberg, and U. T. Eysel, γ-Frequency fluctuations of the membrane potential and response selectivity in visual cortical neurons, Eur. J. Neurosci. **17**, 1768 (2003).

[21] T. Hoch, S. Volgushev, A. Malyshev, K. Obermayer, and M. Volgushev, Modulation of the amplitude of γ-band activity by stimulus phase enhances signal encoding, Eur. J. Neurosci. **33**, 1223 (2011).

[22] C. D. Harvey, F. Collman, D. A. Dombeck, and D. W. Tank, Intracellular dynamics of hippocampal place cells during virtual navigation, Nature **461**, 941 (2009).

[23] S. Mensi, O. Hagens, W. Gerstner, and C. Pozzorini, Enhanced sensitivity to rapid input fluctuations by nonlinear threshold dynamics in neocortical pyramidal neurons, PLoS Comput. Biol. **12**, e1004761 (2016).

[24] M. Arsiero, H.-R. Lüscher, B. N. Lundstrom, and M. Giugliano, The impact of input fluctuations on the frequency–current relationships of layer 5 pyramidal neurons in the rat medial prefrontal cortex, J. Neurosci. **27**, 3274 (2007).

[25] T. Herfurth and T. Tchumatchenko, How linear response shaped models of neural circuits and the quest for alternatives, Curr. Opin. Neurobiol. **46** 234 (2017).

[26] B. Lindner and L. Schimansky-Geier, Transmission of Noise Coded versus Additive Signals through a Neuronal Ensemble, Phys. Rev. Lett. **86**, 2934 (2001).
[27] N. Brunel, F. S. Chance, N. Fourcaud, and L. F. Abbott, Effects of Synaptic Noise and Filtering on the Frequency Response of Spiking Neurons, Phys. Rev. Lett. **86**, 2186 (2001).
[28] N. Fourcaud-Trocmé and N. Brunel, Dynamics of the instantaneous firing rate in response to changes in input statistics, J. Comput. Neurosci. **18**, 311 (2005).
[29] N. Fourcaud and N. Brunel, Dynamics of the firing probability of noisy integrate-and-fire neurons, Neural Comput. **14**, 2057 (2002).
[30] M. J. E. Richardson, Firing-rate response of linear and nonlinear integrate-and-fire neurons to modulated current-based and conductance-based synaptic drive, Phys. Rev. E **76**, 021919 (2007).
[31] N. Brunel, V. Hakim, and M. J. E. Richardson, Single neuron dynamics and computation, Curr. Opin. Neurobiol. **25**, 149 (2014).
[32] S. Ostojic, G. Szapiro, E. Schwartz, B. Barbour, N. Brunel, and V. Hakim, Neuronal morphology generates high-frequency firing resonance, J. Neurosci. **35**, 7056 (2015).
[33] J. Doose, G. Doron, M. Brecht, and B. Lindner, Cellular/molecular noisy juxtacellular stimulation *in vivo* leads to reliable spiking and reveals high-frequency coding in single neurons, J. Neurosci. **36**, 11120 (2016).
[34] G. Testa-Silva, M. B. Verhoog, D. Linaro, C. P. J. de Kock, J. C. Baayen, R. M. Meredith, C. I. De Zeeuw, M. Giugliano, and H. D. Mansvelder, High bandwidth synaptic communication and frequency tracking in human neocortex, PLoS Biol. **12**, e1002007 (2014).
[35] A. Borst and F. E. Theunissen, Information theory and neural coding, Nat. Neurosci. **2**, 947 (1999).
[36] F. Rieke, D. A. Bodnar, and W. Bialek, Naturalistic stimuli increase the rate and efficiency of information transmission by primary auditory afferents, Proc. R. Soc. A **262**, 259 (1995).
[37] A. B. Neiman and D. F. Russell, Sensory coding in oscillatory electroreceptors of paddlefish, Chaos **21**, 047505 (2011).
[38] R. D. Vilela and B. Lindner, Comparative study of different integrate-and-fire neurons: Spontaneous activity, dynamical response, and stimulus-induced correlation, Phys. Rev. E **80**, 031909 (2009).
[39] S. G. Sadeghi, M. J. Chacron, M. C. Taylor, and K. E. Cullen, Neural variability, detection thresholds, and information transmission in the vestibular system, J. Neurosci. **27**, 771 (2007).
[40] S. Blankenburg, W. Wu, B. Lindner, and S. Schreiber, Information filtering in resonant neurons, J. Comput. Neurosci. **39**, 349 (2015).
[41] H. Clague, F. Theunissen, and J. P. Miller, Effects of adaptation on neural coding by primary sensory interneurons in the cricket cercal system, J. Neurophysiol. **77**, 207 (1997).
[42] C. Pozzorini, R. Naud, S. Mensi, and W. Gerstner, Temporal whitening by power-law adaptation in neocortical neurons, Nat. Neurosci. **16**, 942 (2013).
[43] M. N. Shadlen and W. T. Newsome, The variable discharge of cortical neurons: Implications for connectivity, computation, and information coding, J. Neurosci. **18**, 3870 (1998).
[44] C. van Vreeswijk and H. Sompolinsky, Chaos in neuronal networks with balanced excitatory and inhibitory activity, Science **274**, 1724 (1996).
[45] A. Dettner, S. Münzberg, and T. Tchumatchenko, Temporal pairwise spike correlations fully capture single-neuron information, Nat. Commun. **7**, 13805 (2016).
[46] N. Fourcaud-Trocmé, D. Hansel, C. Van Vreeswijk, and N. Brunel, How spike generation mechanisms determine the neuronal response to fluctuating inputs, J. Neurosci. **23**, 11628 (2003).
[47] B. B. Averbeck, P. E. Latham, and A. Pouget, Neural correlations, population coding and computation, Nat. Rev. Neurosci. **7**, 358 (2006).
[48] B. Lindner, M. J. Chacron, and A. Longtin, Integrate-and-fire neurons with threshold noise: A tractable model of how interspike interval correlations affect neuronal signal transmission, Phys. Rev. E **72**, 021911 (2005).
[49] L. Badel, S. Lefort, R. Brette, C. C. H. Petersen, W. Gerstner, and M. J. E. Richardson, Dynamic iv curves are reliable predictors of naturalistic pyramidal-neuron voltage traces, J. Neurophysiol. **99**, 656 (2008).
[50] F. R. Fernandez, P. Malerba, and J. A. White, Non-linear membrane properties in entorhinal cortical stellate cells reduce modulation of input-output responses by voltage fluctuations, PLoS Comput. Biol. **11**, e1004188 (2015).
[51] S. Ostojic, N. Brunel, and V. Hakim, How connectivity, background activity, and synaptic properties shape the cross-correlation between spike trains, J. Neurosci. **29**, 10234 (2009).
[52] F. Gabbiani, Coding of time-varying signals in spike trains of linear and half-wave rectifying neurons, Network: Computation in Neural Systems **7**, 61 (1996).
[53] J. C. Roddey, B. Girish, and J. P. Miller, Assessing the performance of neural encoding models in the presence of noise, J. Comput. Neurosci. **8**, 95 (2000).
[54] M. H. Rowe and A. B. Neiman, Information analysis of posterior canal afferents in the turtle, *Trachemys scripta elegans*, Brain Res. **1434**, 226 (2012).
[55] D. R. Chialvo, A. Longtin, and J. Müller-Gerking, Stochastic resonance in models of neuronal ensembles, Phys. Rev. E **55**, 1798 (1997).
[56] S. O. Voronenko and B. Lindner, Weakly nonlinear response of noisy neurons, New J. Phys. **19**, 033038 (2017).
[57] D. T. Gillespie, Exact numerical simulation of the ornstein-uhlenbeck process and its integral, Phys. Rev. E **54**, 2084 (1996).
[58] A. Destexhe, M. Rudolph, and D. Paré, The high-conductance state of neocortical neurons *in vivo*, Nat. Rev. Neurosci. **4**, 739 (2003).
[59] A. Rauch, G. La Camera, H.-R. Lüscher, W. Senn, and S. Fusi, Neocortical pyramidal cells respond as integrate-and-fire neurons to *in vivo*–like input currents, J. Neurophysiol. **90**, 1598 (2003).
[60] A. S. Ecker, P. Berens, G. A. Keliris, M. Bethge, N. K. Logothetis, and A. S. Tolias, Decorrelated neuronal firing in cortical microcircuits, Science **327**, 584 (2010).
[61] A. Renart, J. De La Rocha, P. Bartho, L. Hollender, N. Parga, A. Reyes, and K. D. Harris, The asynchronous state in cortical circuits, Science **327**, 587 (2010).
[62] L. G. Nowak, R. Azouz, M. V. Sanchez-Vives, C. M. Gray, and D. A. McCormick, Electrophysiological classes of cat primary visual cortical neurons *in vivo* as revealed by quantitative analyses, J. Neurophysiol. **89**, 1541 (2003).

[63] J. Pressley and T. W. Troyer, Complementary responses to mean and variance modulations in the perfect integrate-and-fire model, Biol. Cybern. **101**, 63 (2009).

[64] S. Ostojic, Inter-spike interval distributions of spiking neurons driven by fluctuating inputs, J. Neurophysiol. **106**, 361 (2011).

[65] P. F. Craigmile, Simulating a class of stationary gaussian processes using the davies–harte algorithm, with application to long memory processes, J. Time Ser. Anal. **24**, 505 (2003).

[66] H. Ko, L. Cossell, C. Baragli, J. Antolik, C. Clopath, S. B. Hofer, and T. D. Mrsic-Flogel, The emergence of functional microcircuits in visual cortex, Nature **496**, 96 (2013).

[67] G. Maimon and J. A. Assad, Beyond poisson: Increased spike-time regularity across primate parietal cortex, Neuron **62**, 426 (2009).

[68] J. de la Rocha, B. Doiron, E. Shea-Brown, K. Josić, and A. D. Reyes, Correlation between neural spike trains increases with firing rate, Nature **448**, 802 (2007).

[69] http://www.tchumatchenko.de/source_code_nov18.zip.

[70] A. Y. Y. Tan, Spatial diversity of spontaneous activity in the cortex, Front. Neur. Circ. **9**, 48 (2015).

[71] M. C. Angulo, J. Rossier, and E. Audinat, Postsynaptic glutamate receptors and integrative properties of fast-spiking interneurons in the rat neocortex, J. Neurophysiol. **82**, 1295 (1999).

[72] A. C. Flint, U. S. Maisch, J. H. Weishaupt, A. R. Kriegstein, and H. Monyer, Nr2a subunit expression shortens NMDA receptor synaptic currents in developing neocortex, J. Neurosci. **17**, 2469 (1997).

[73] P. Khorsand and F. Chance, Transient responses to rapid changes in mean and variance in spiking models, PloS ONE **3**, e3786 (2008).

[74] M. J. Chacron, Nonlinear information processing in a model sensory system, J. Neurophysiol. **95**, 2933 (2006).